A Novel Beam-Steerable Antenna Using HIS-SWG Reconfigurable Artificial Ground Structure

You-Feng Cheng [1], Xiao Ding [2], Wei Shao [2], and Cheng Liao [1]

[1] Institute of Electromagnetics
Southwest Jiaotong University, Chengdu 610031, China
juvencheng1377@gmail.com, c.liao@swjtu.edu.cn

[2] Institute of Applied Physics
University of Electronic Science and Technology of China, Chengdu, 610054, China
xding@uestc.edu.cn, weishao@uestc.edu.cn

Abstract ─ An artificial ground structure (AGS) which can be switched between the high-impedance surface (HIS), the surface-waveguide (SWG) and the HIS-SWG hybrid structure is proposed for the design of a beam-steerable antenna. The AGS is reconfigured with PIN diodes inserted on the bottom ground. The antenna radiates a broadside far-field pattern when the AGS is reconfigured into an HIS, and it steers its main beam to the endfire direction when the AGS exhibits as an HIS-SWG hybrid structure. The reconfigured HIS and SWG are analyzed using the Brillouin dispersion theory and the eigenvalue analysis, respectively. A prototype of the proposed beam-steerable antenna is fabricated and measured. The measured results including the reflection coefficients and radiation patterns validate the antenna performance.

Index Terms ─ Artificial ground structure (AGS), beam-steerable antenna, eigenvalue analysis, high-impedance surface (HIS), surface-wave guide (SWG).

I. INTRODUCTION

The rapid development of modern communication systems has shown the increasing demand of multi-functional antennas which are capable of achieving more than one operational status by electronic or mechanical implementation. Reconfigurable antennas are attractive and effective solutions [1-3]. As one versatile type of reconfigurable antennas, the beam-steerable antenna can dynamically switch its radiation pattern with other antenna characteristics unchanged. Generally, for many practical applications, it is required that the beam-steerable antenna should have a good gain flatness between the radiation patterns of different modes, a wide combined main-beam coverage and a powerful reconfigurable ability. These rigorous but essential requirements have brought great challenges to the designs of beam-steerable antennas.

The beam-steerable antenna can be realized by various solutions, such as reconfiguring its parasitic structures [4-8], reconfiguring its feeding networks [9-11], and reconfiguring its radiator loads [12]. In [8], a beam-steerable antenna based on a dual-reconfiguration technique was proposed. The reconfigured strips on the lower layer realize a preliminary beam control, and the parasitic pixel structure is exploited to further increase the beam-steerable ability. Recently, many efforts have been devoted to the design of beam-steerable antennas based on meta-materials [13-15]. In [14], a high-impedance surface (HIS) was designed to propagate the TE Floquet mode in the given frequency band, and a surface-wave assistant antenna based on the HIS was proposed to achieve reconfigurable radiation patterns.

In this paper, a novel beam-steerable antenna based on the artificial ground structure (AGS) is presented. Firstly, the proposed AGS is designed and analyzed to have the capability of being switched between the HIS, the surface-wave-guide (SWG) and the HIS-SWG hybrid structure. Then, a dipole is placed upon the AGS and it can steer its far-filed pattern from a broadside radiation with an HIS to an end-fire radiation with an HIS-SWG hybrid structure. At last, a prototype of the proposed antenna is fabricated and measured, and the measured results show good gain flatness and wide combined-beam coverage.

II. AGS DESIGN AND ANALYSIS

In order to realize the HIS-SWG reconfiguration at a selected operation frequency, the AGS is required to meet two conditions simultaneously. On one hand, the reconfigured HIS should form a forbidden frequency band-gap which contains the operation frequency, and on the other hand, the reconfigured SWG is able to support the propagation of required surface waves at the same frequency.

The geometries of the HIS and SWG reconfigured

Submitted On: February 25, 2018
Accepted On: December 25, 2018

1054-4887 © ACES

from the AGS are shown in Fig. 1. The mushroom-shaped HIS [16] consists of 5 × 5 square units, which have a size of $D_H \times D_H$. The square patches with a length of L_c are periodically printed on the top of a substrate. Vertical metal vias with a diameter of D_c connect the upper square patches to the ground plane. The substrate has a relative permittivity of 2.95 and a height of H_2. The structure of the proposed SWG is the same as the HIS except for the ground plane, which are also pixelated as 5 × 5 square patches. Thus, the upper and lower surfaces of the SWG are the same.

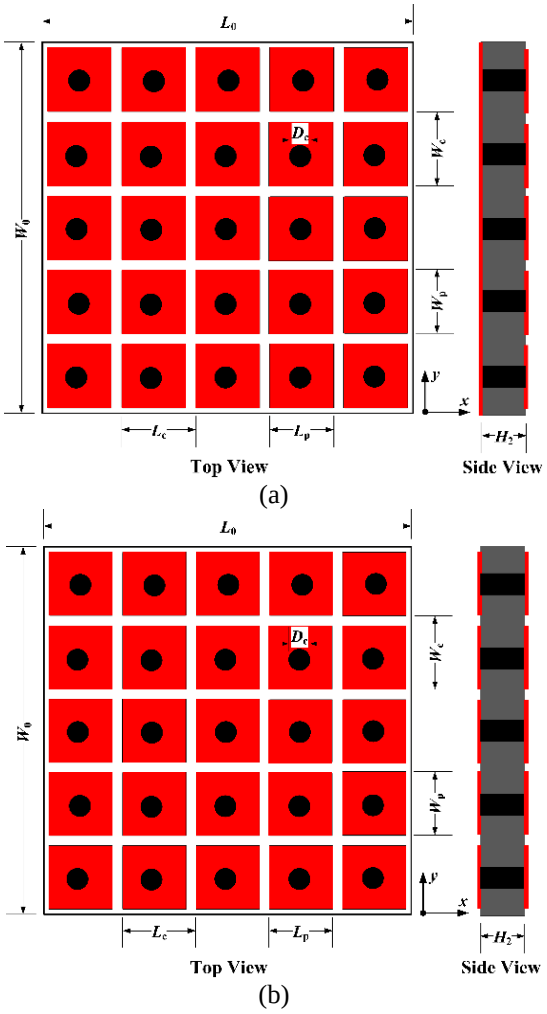

Fig. 1. Structures of the reconfigured HIS and SWG. (a) Mushroom-shaped HIS, and (b) designed SWG.

The HIS unit cell can be equivalent as a series LC circuit in which the major contribution to the overall capacity (C_g) comes from the gap discontinuity at both ends of the patch, and the overall inductance (L_c) comes from the current loop through the vias and the ground plane. Thus, there exists a resonance according to the LC circuit, and the equivalent sheet impedance at the resonant frequency can be calculated by:

$$Z = \frac{j\omega L_c}{1-\omega^2 L_c C_g}, \tag{1}$$

where ω is the angular frequency, and the resonant frequency is:

$$\omega_0 = \frac{1}{\sqrt{L_c C_g}}. \tag{2}$$

It can be seen from (1) and (2) that the surface impedance is very high near the resonant frequency. Thus, a forbidden frequency band-gap is formed. The simulated dispersion diagrams of the proposed HIS are shown in Fig. 2. It can be observed that there exists a complete band-gap between the first and second modes which is centered at 4.5 GHz and spans from 3.43 to 5.42 GHz.

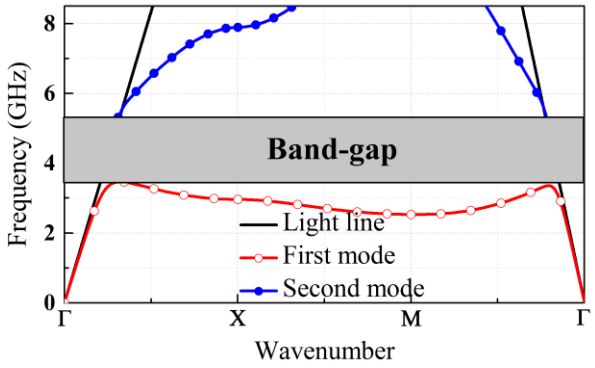

Fig. 2. Dispersion diagram of the reconfigured HIS.

The band-gap would disappear when the ground plane is also pixelated as square patches. In terms of the reconfigured SWG, the Snell's law, effective surface impedance and eigenvalue analysis are used to illustrate that it can support the propagation of TE_0- and TM_0-mode surface waves.

Firstly, the propagation of the surface wave in the proposed SWG can be explained with the Snell's law:

$$n_1 \cdot \sin\theta_1 = n_2 \cdot \sin\theta_2. \tag{3}$$

Equation (3) means that the refraction angle θ_2 would get larger with the increase of the refractive index of the SWG as shown in Fig. 3. Thus, the total reflection may be realized when the refractive index is large enough. The real part of the refractive index of the SWG can be calculated from the simulated S-parameters, and the transform can be given as [17]:

$$n_{\text{eff}} = \frac{1}{k_0 L_c}\cos^{-1}\left[\frac{1}{2S_{21}}(1-S_{11}^2+S_{21}^2)\right], \tag{4}$$

where k_0 is the wavenumber of the incident wave in free space. The calculated refractive index is shown in Fig. 4 (a). It can be observed that the SWG has a significant portion of the calculated real part of n_{eff} at a selected

frequency (3.6 GHz). Therefore, the surface wave can propagate in the proposed SWG.

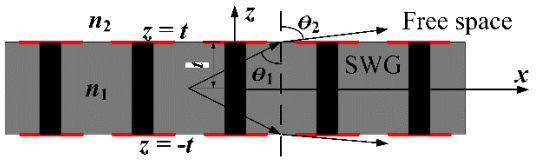

Fig. 3. Sketch map of electromagnetic wave transmission.

Secondly, the relative surface impedance Z_s of the SWG can also be calculated from the simulated S-parameters [18], and the transform is given as:

$$Z_s = \pm\sqrt{\frac{(1+S_{11})^2 - S_{21}^2}{(1-S_{11})^2 - S_{21}^2}}\,. \tag{5}$$

Since the SWG is a passive medium, the sign in (5) should satisfy the requirement that the real part of the relative impedance should be positive. The calculated relative surface impedance is also plotted in Fig. 4 (a). It can be seen that, at 3.6 GHz, the imaginary part of the surface impedance is zero and the real part is close to the free-space wave impedance, which indicates that the proposed SWG is matched to the free space. According to [19], the dielectric SWG can support both the TE- and TM-mode surface waves.

At last, the solution of eigenvalues is utilized to explain that the selection of the SWG height makes it only guide surface waves of TE_0 and TM_0 modes. According to [19], the eigenvalue equations are:

$$\begin{cases} \varepsilon_r pt = ht\tan ht & \text{TM even modes} \\ \varepsilon_r pt = -ht\cot ht & \text{TM odd modes} \\ pt = ht\tan ht & \text{TE even modes} \\ pt = -ht\cot ht & \text{TE odd modes} \end{cases}, \tag{6}$$

where ε_r is the relative dielectric constant which can be calculated by the refractive index in (4), *ht* and *pt* are two eigenvalues from the geometry and boundary condition, $t = H_2/2$. *h* and *p* are the cutoff wavenumber of the air and the SWG, respectively, and they satisfy:

$$\begin{cases} (pt)^2 + (ht)^2 = (\varepsilon_r - 1)(k_0 t)^2 \\ \beta^2 = k_0^2 + p^2 = \varepsilon_r k_0^2 - h^2 \end{cases}. \tag{7}$$

According to (6) and (7), the solution of eigenvalues of the SWG can be illustrated in Fig. 4 (b). It can be deduced that only the TE_0 and TM_0 modes are guaranteed to propagate and other higher-order modes are rapidly attenuated since there is almost no intersection between the quarter-circle with a radius of $R = (\varepsilon_r - 1)^{1/2} k_0 t = 0.52$ and the eigen-functions of higher order modes.

Based on the above analysis, it can be indicated that the proposed AGS can forbidden the propagation of TE_0- and TM_0-mode surface waves when it is reconfigured into an HIS, and it can guide these surface waves to a selected direction when it is partly switched into an HIS and partly into an SWG.

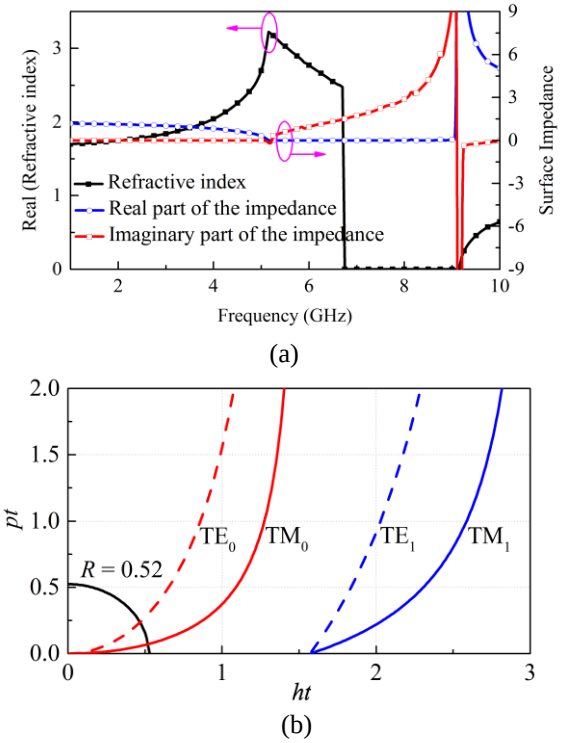

Fig. 4. Calculated real part of the refractive index, relative surface impedance and solution of eigenvalues. (a) Real part of the refractive index and relative surface impedance, and (b) solution of eigenvalues.

Infineon's BAR64-02V PIN diodes are used to reconfigure the AGS. As shown in Fig. 5, the square patches on the bottom of the substrate are divided into three groups, namely Groups 1, 2 and 3. When the AGS operates at Mode 1, the square patches of Group 2 are all connected. In this situation, the AGS exhibits as an HIS-SWG hybrid structure, and the surface waves can only propagate to the negative *x* direction. Similarly, when the AGS operates at Mode 2, the square patches of Group 3 are all connected. The AGS is also an HIS-SWG hybrid structure in this situation and the surface waves can only propagate to the positive *x* direction. When the square patches of Groups2 and 3 are all connected, the surface works as an HIS, and this case is denoted as Mode 3. Herein no surface waves can be supported in this case. The bias circuits are also shown in Fig. 5. Note that the bias circuits have small effects on the AGS performance since they are placed on the back side of the substrate.

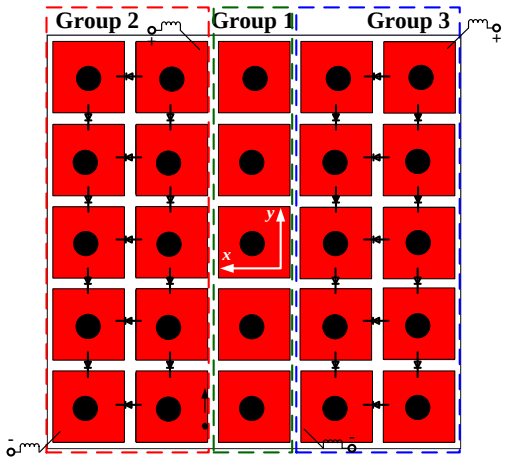

Fig. 5. Back side of the AGS and its bias circuits.

III. BEAM-STEERABLE ANTENNA DESIGN AND EXPRIMENT VALIDATION

A beam-steerable antenna is designed based on the proposed AGS as plotted in Fig. 6. A symmetric dipole is printed on the upper substrate which is placed on the AGS. The substrate has a thickness of H_1 and a relative permittivity of 2.2. To provide the excitation of the antenna, a coaxial probe penetrates the lower and upper substrates and connects to one side of the dipole. The other side of the dipole is shorted to the back side of the artificial surface with a shorting pin, which has a same radius with that of the coaxial inner conductor. In addition, two slots with a radius of 2.3 times of the radius of the coaxial inner conductor are etched on the artificial surface. The antenna is designed to operate at 3.6 GHz. The optimized parameters are: $L_0 = W_0 = 45$ mm, $L_c = W_c = 9$ mm, $L_p = W_p = 7.8$ mm, $L_d = 19.2$ mm, $W_d = 1.5$ mm, $D_f = 3.2$ mm, $D_s = 1.2$ mm, $D_v = 0.2$ mm, $H_1 = 0.508$ mm and $H_2 = 3$ mm.

The simulated E- and H-field distributions of the antenna are depicted in Fig. 7. Since TE_0-mode surface waves only exist the E_y component while TM_0-mode surface waves exist the E_x and E_z components, it can be indicated from Fig. 7 that the excited surface waves are of TE_0 mode.

The explanations of the beam-steering principles are given as follows. When the AGS operates at Mode 1, the propagation of the surface wave toward the positive x-direction is forbidden and that toward the negative x-direction is supported. Thus, an endfire radiation tilted to the negative x-direction is generated. When the AGS operates at Mode 2, the situation is exactly opposite to Mode 1, and an endfire pattern tilted to the positive x-direction is radiated. When the AGS operates at Mode 3, an HIS-based antenna is obtained, and it generates a broadside radiation. Therefore, the antenna is able to steer its far-filed pattern from a broadside radiation with an HIS ground to an end-fire radiation with an HIS-SWG hybrid ground.

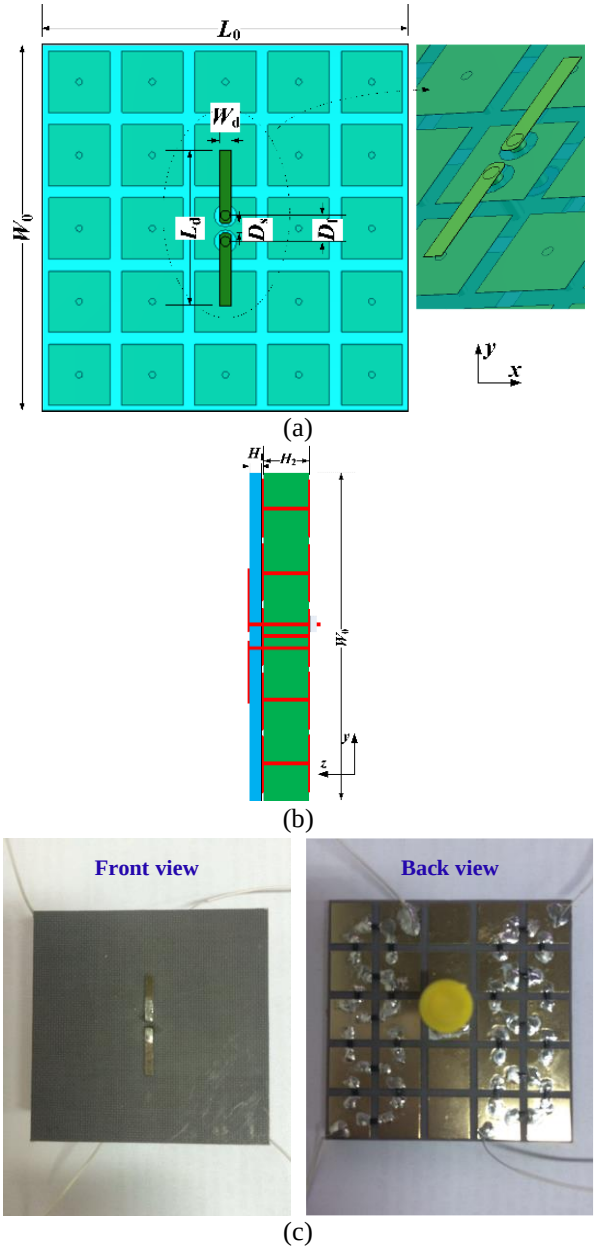

Fig. 6. Antenna geometry and its fabricated prototype sample. (a) Front view, (b) side view, and (c) prototype.

The antenna is fabricated and measured, and the fabricated prototype is shown in Fig. 6 (c). Figure 8 plots the simulated and measured input performance in terms of S_{11}. From the curves of the reflection coefficients, the two modes have a common bandwidth of 3.53 – 3.78 GHz with S_{11} below -10 dB. It should be noted that the results of Mode 2 are omitted due to the geometry symmetry between Modes 2 and 3.

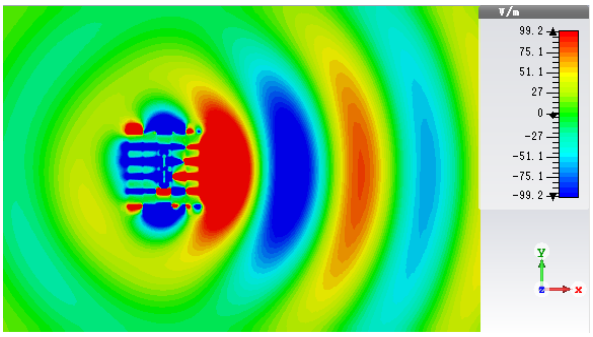

(a)

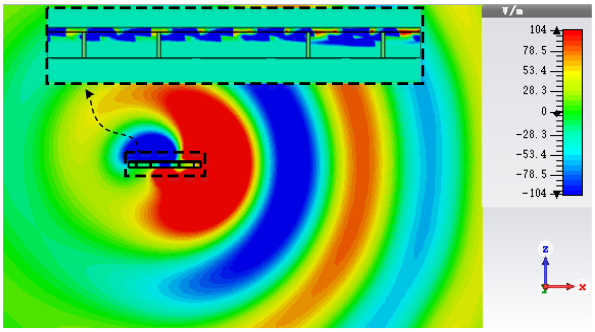

(b)

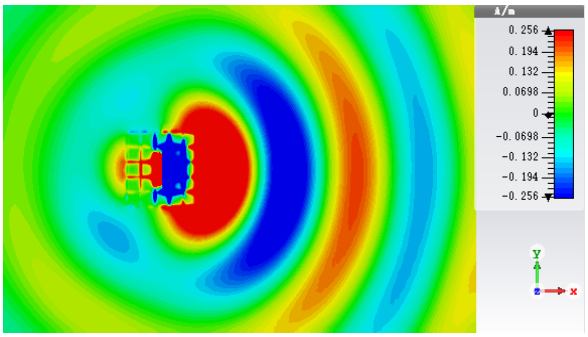

(c)

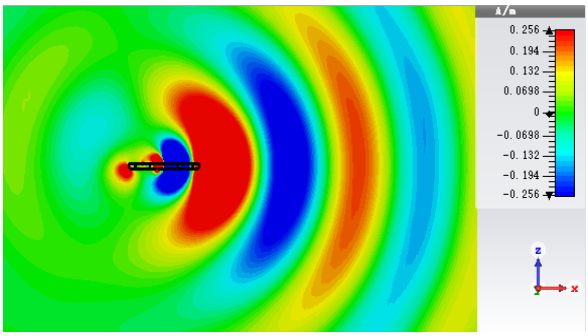

(d)

Fig. 7. Simulated E_y and H_z distributions: (a)-(b) E_y distribution on the vertical observation plane z = 3.6 mm and the horizontal observation plane y = 0 mm. (c)-(d) H_z distribution on the vertical observation plane z = 3.6 mm and the horizontal observation plane y = 0 mm.

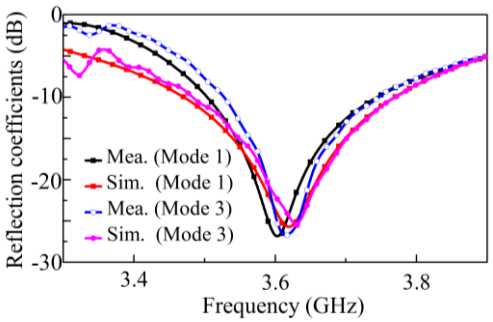

Fig. 8. Measured and simulated return losses of the beam-steerable antenna.

The antenna resonance is determined by the AGS and the length of the above dipole. When the beam-steerable antenna radiates an endfire pattern, the radiation aperture is one edge of the SWG. In this situation, the SWG size determines the resonant frequency and the dipole determines should excite surface waves at the frequency. When the antenna generates a broadside radiation, the dipole becomes the radiation source. In this case, the dipole length determines the antenna resonance. In order to validate the above description, here some comparisons and parametric studies are carried out. Firstly, when the AGS is reconfigured into an HIS, the antenna reflection performance with different dipole lengths is studied. As shown in Fig. 9 (a), with the increase of the dipole length, the antenna resonance is shifted downwards to the lower frequency band. Besides, the antenna resonant performance has no deterioration with the change of the dipole length. Secondly, when the AGS is switched into an HIS-SWG hybrid structure, the influence of the SWG size on the reflection coefficients is investigated and shown in Fig. 9 (b). It can be found that the resonant frequency decreases when the SWG cells increases form 3×3 to 7×7. In addition, the resonant performance deteriorates when the SWG size is changed. The reason is there is a discrepancy between the resonant frequency of surface waves excited by the dipole and the resonance radiated by the SWG edge.

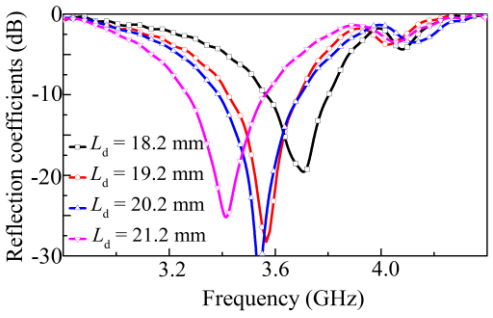

(a)

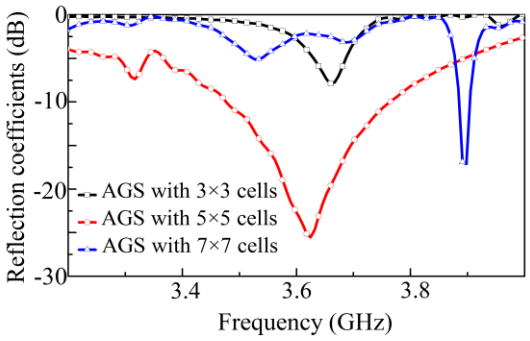

(b)

Fig. 9 Simulated |S11| curves with different dipole lengths and SWG sizes. (a) With different dipole lengths when the AGS works as an HIS, and (b) with different SWG sizes when the AGS works as an HIS-SWG hybrid structure.

The reconfigured patterns at these three modes are listed in Fig. 10. The far-field patterns are measured in an anechoic chamber with a SATIMO Antenna Measurement System. Figure 11 illustrates the measured and simulated radiation patterns and polarization information of the proposed antenna in the *xoz* plane. In Fig. 11 (a), when the antenna operates at Mode 1, it radiates a broadside beam with a measured gain of 5.2 dBi. When the antenna operates at Mode 3, it has an end-fire radiation beam pointing to θ_{max}= -90° direction as shown in Fig. 11 (b). The measured gain at Mode 3 is 4.9 dBi, which is a little lower than that at Mode 1. The half-power beamwidths at Modes 1 and 3 are 96° and 118°, respectively. Based on the symmetry of the Modes 2 and 3, it can be indicated that the proposed reconfigurable antenna is able to switch its main beam to cover the above half space.

Figure 12 shows the measured efficiencies at Modes 1 and 3, which are the total efficiencies defined as the ratio of the radiated power from the antenna to the input power to the antenna. It can be observed that the measured efficiencies of the both modes are about 90% at the resonant frequency. The reason why the measured efficiencies are quite high can be addressed from two aspects. Firstly, Infineon's BAR64-02V PIN diodes are adopted to the antenna design. According to its datasheet, the insertion loss of this diode is about 0.05 dB, which means the inserted PIN diodes bring only a small amount of loss. Secondly, all these PIN diodes are placed on the lower layer of the AGS. When the AGS works as an HIS, the PIN diodes are placed on the ground plane and they lead low loss into the design, which has been described in [20]. When the AGS works as an HIS-SWG hybrid structure, high-frequency surface waves are bounded into the SWG and the current doesn't flow through the PIN diodes. In addition, all the PIN diodes are switched off when the AGS works as an SWG.

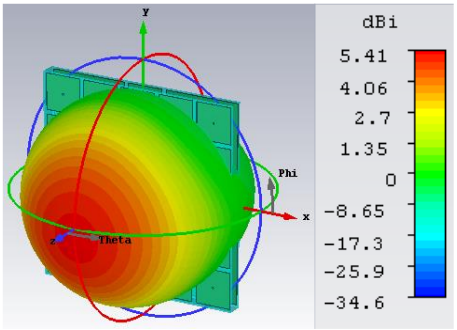

(a)

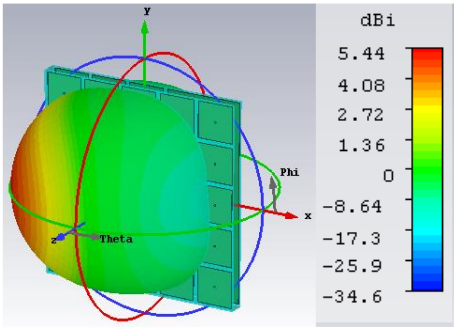

(b)

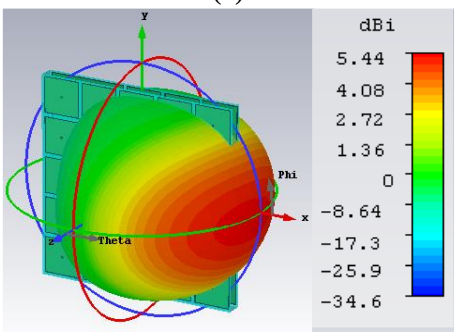

(c)

Fig. 10. Simulated 3-D reconfigurable patterns of the antenna. (a) Broadside pattern, and (b)-(c) endfire patterns.

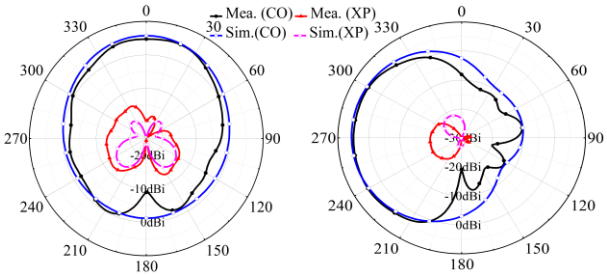

(a) (b)

Fig. 11. Measured and simulated radiation patterns of the beam-steerable antenna. (a) Mode 1 and (b) Mode 3.

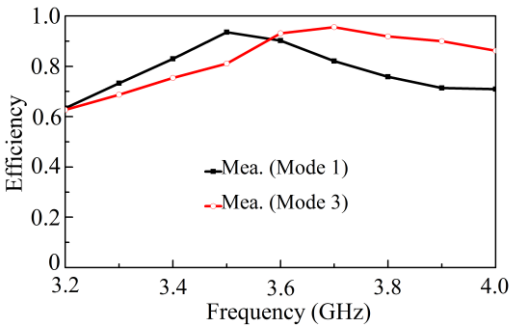

Fig. 12. Measured efficiencies of the proposed antenna when it works at Modes 1 and 3.

IV. CONCLUSION

In this work, a beam-steerable antenna based on the HIS-SWG AGS is presented. Firstly, an AGS which can be switched between the HIS, SWG and HIS-SWG hybrid surface is designed. The switching is realized by PIN diodes. Then, a dipole is located above the AGS for beam steering. When the AGS works as an HIS, a broadside radiation is obtained. An end-fire main beam can be generated when the AGS works as an HIS-SWG hybrid structure. At last, a prototype is fabricated and measured, and the measured results agree well with the simulated ones. The measured results also validate the beam-steering performance of the antenna.

ACKNOWLEDGMENT

This work was supported by the National Natural Science Foundation of China (Grants No. 61731005, No. 61771407 and No. 61801405) and Aeronautical Science Foundation of China (ASFC-20162080008).

REFERENCES

[1] J. Bernhard, E. Bonek, C. G. Christodoulou, D. Kunkee, and K. L. Melde, "Guest editorial for the special section on antenna systems and propagation for cognitive radio," *IEEE Trans. Antennas Propagat.*, vol. 62, no. 3, pp. 1015-1018, Mar. 2014.

[2] C. G. Christodoulou, Y. Tawk, S. A. Lane, and S. R. Erwin, "Reconfigurable antennas for wireless and space applications," *Proc. IEEE*, vol. 100, no. 7, pp. 2250-2261, July 2012.

[3] N. Ojaroudi, Y. Ojaroudi, S. Ojaroudi, Y. Ebazadeh, and M. Shirgir, "Small reconfigurable monopole antenna integrated with PIN diodes for multimode wireless communications," *Applied Computational Electromagnetics Society Journal*, vol. 29, no. 7, pp. 541-546, July 2014.

[4] S. Zhang, G. H. Huff, J. Feng, and J. T. Bernhard, "A pattern reconfigurable microstrip parasitic array," *IEEE Trans. Antennas Propagat.*, vol. 52, pp. 2773-2776, Oct. 2004.

[5] J. Zhang, X. S. Yang, J. L. Li, and B. Z. Wang, "Triangular patch Yagi antenna with reconfigureable pattern characteristics," *Applied Computational Electromagnetics Society Journal*, vol. 27, no. 11, pp. 541-546, Nov. 2012.

[6] D. Rodrigo and L. Jofre "Frequency and radiation pattern reconfigurability of a multi-size pixel antenna," *IEEE Trans. Antennas Propagat.*, vol. 60, no. 5, pp.2219-2225, 2012.

[7] D. Rodrigo, B. A. Cetiner, and L. Jofre, "Frequency, radiation pattern and polarization reconfigurable antenna using a parasitic pixel layer," *IEEE Trans. Antennas Propagat.*, vol. 62, no. 6, pp. 3422-3427, June 2014.

[8] Y. F. Cheng, W. Shao, X. Ding, and et.al., "A novel beam steerable antenna based ondual-reconfiguration technique," *J. Electromagn Waves Appl.*, vol. 31, no. 7, pp. 740-751, Apr. 2017.

[9] X. Ding and B.-Z. Wang, "A millimeter-wave pattern-reconfigurable antenna with a reconfigurable feeding network," *J. Electromagn. Waves Applicat.*, vol. 27, no. 5, pp. 649-658, Jan. 2013.

[10] X. Jiang, Z. Zhang, Y. Li, and Z. Feng, "A novel null scanning antenna using even and odd modes of a shorted patch," *IEEE Trans. Antennas Propag.*, vol. 62, no. 4, pp. 1903-1909, Apr. 2014.

[11] Y. F. Cheng, X. Ding, B. Z. Wang, and W. Shao, "An azimuth-pattern-reconfigurable antenna with enhanced gain and front-to-back ratio," *IEEE Antennas Wireless Propag. Lett.*, vol. 16, pp. 2303-2306, Aug. 2017.

[12] W. H. Chen and Z. H. Feng, "Planar reconfigurable pattern antenna by reactive-load switching," *Microw. Opt. Technol. Lett.*, vol. 47, no. 5, pp. 506-507, Dec. 2005.

[13] P. Deo, A. Mehta, D. Mirshekar-Syahkal, and H. Nakano, "An HIS based spiral antenna for pattern reconfigurable applications," *IEEE Antennas Wireless Propag. Lett.*, vol. 8, pp. 196–199, 2009.

[14] J. Ren, X. Yang, J. Yin, and Y. Yin, "A novel antenna with reconfigurable patterns using H-shaped structures," *IEEE Antennas Wireless Propag. Lett.*, vol. 14, pp. 915-918, 2015.

[15] M. Li, S. Q. Xiao, Z. Wang, and B. Z. Wang, "Compact surface-wave assisted beam-steerable antenna based on HIS," *IEEE Trans. Antennas Propag.*, vol. 62, no. 7, pp. 3511-3519, July 2014.

[16] D. Sievenpiper, L. J. Zhang, Romulo, F. J. Broas, N. G. Alexopolaus, and E. Yablonovitch, "High-impedance electromagnetic surfaces with a forbidden frequency band," *IEEE Microwave Theory Tech.*, vol. 47, no. 11, pp. 2059-2074, Nov. 1999.

[17] D. R. Smith, D. C. Vier, T. Koschny, and C. M. Soukoulis, "Electromagnetic parameter retrieval from inhomogeneous metamaterials," *Phys. Rev. E*, vol. 71, p. 036617, Mar. 2005.

[18] X. D. Chen, T. M. Grzegorczyk, B. I. Wu, J. Pacheco, and J. A. Kong, "Robust method to retrieve the constitutive effective parameters of metamaterials," *Phys. Rev. E*, vol. 70, p. 016608, July 2004.
[19] R. E. Collin, *Field Theory of Guided Waves*. 2nd edition, New York: IEEE Press, 1991.
[20] B. Majumda and K. P. Esselle, "Fixed frequency broadside–endfire beam steerable antennas," *Electro. Lett.*, vol. 52, no. 15, pp. 1282-1284, July 2016.

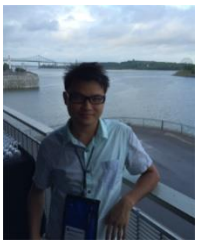

You-Feng Cheng was born in Anhui, China, in 1989. He received the Ph.D. degree in Radio Physics from the University of Electronic Science and Technology of China (UESTC), Chengdu, China, in 2018. In 2017, he was a Visiting Scholar with the Mechanical Engineering Department, University of Houston, Houston, TX, USA. He joined Southwest Jiaotong University (SWJTU), Chengdu, China, in 2018. His research interests include phased arrays, reconfigurable antennas, and evolutionary algorithms.

Xiao Ding received the B.S. and M.S. degrees in Electronic Engineering, from Guilin University of Electronic Science and Technology (GUET), Guilin, China, and the Ph.D. degree in Radio Physics from University of Electronic Science and Technology of China (UESTC), Chengdu, China, in 2014. He joined the UESTC in 2014, where he is currently an Associate Professor. In 2013, he was a Visiting Scholar at the South Dakota School of Mines and Technology, SD, USA. From June 2016 to June 2017, he was a Visiting Scholar at the University of Houston, TX, USA. His research interests include reconfigurable antennas and its' applications and phased arrays.

Wei Shao received the M.Sc. and Ph.D. degrees in Radio Physics from UESTC, Chengdu, China, in 2004 and 2006, respectively. He joined the UESTC and is now a Professor. He has been a Visiting Scholar in the Electromagnetic Communication (CEM) Laboratory, Pennsylvania State University in 2010. His research interests include computational electromagnetics and antenna design.

Cheng Liao was born in Chongqing, China, in 1964. He received the Ph.D. degree in Electromagnetic Fields and Microwave Techniques from the University of Electronic Science and Technology of China (UESTC), Chengdu, China, in 1995. From 1997 to 1998, he was a Visiting Scholar at the City University of Hong Kong, Kowloon Tong, Hong Kong. He became a Professor at Southwest Jiaotong University, Chengdu, China, in 1998. His research interests include computational electromagnetic, electromagnetic compatibility, and antenna theory and design.